Relaxation Dynamics of the Hydrated Electron: Femtosecond Time-Resolved Resonance Raman and Luminescence Study

Misao Mizuno,† Shoichi Yamaguchi, and Tahei Tahara*

Molecular Spectroscopy Laboratory, RIKEN (The Institute of Physical and Chemical Research), 2-1 Hirosawa, Wako, Saitama 351-0198, Japan

Received: February 17, 2005; In Final Form: April 24, 2005

Femtosecond time-resolved resonance Raman measurements were carried out to examine the relaxation process of the hydrated electron in water. The rise of the intra- and intermolecular vibrational Raman bands of the solvating water molecules was successfully time-resolved with a time resolution as high as 250 fs. The temporal intensity change of Raman bands, as well as that of luminescence background, was compared with the time evolution of the transient absorption signal. It was found that (1) the Raman and luminescence signals exhibited the same temporal behavior, (2) the rise time of the Raman bands is faster than the appearance of the equilibrated hydrated electron, indicating that the precursor state also gives rise to resonance Raman signals, and (3) the rise of the transient Raman band is slower than that of the transient absorption at the probe wavelength of 800 nm. Because it has been shown that the Raman intensity enhancement arises from the resonance with the s → p transition, fact 2 implies that the precursor state is the nonequilibrated s-state electron. The delayed rise of the Raman signal compared to the absorption was explained in terms of the temporal change of the resonance condition. In very early time when the absorption is largely red-shifted, the probe at 800 nm is resonant with the high energy part of the absorption that provides little resonance Raman enhancement. This explanation was consistent with the probe wavelength dependence of the temporal behavior of the Raman signal: the Raman bands measured with the higher energy probe (600 nm) rose even more slowly. The resonance Raman signal in the anti-Stokes side was also examined, but no anti-Stokes band was observable. It suggests that the temperature increase of the solvation structure around the nonequilibrated hydrated electron is less than 100 K.

1. Introduction

The hydrated electron is the most basic anion in solution and it has been attracting much interest for decades in the fields of chemistry, physics, and biology. A large number of spectroscopic studies have been done so far and, especially, time-resolved absorption experiments were carried out to clarify the relaxation dynamics of the hydrated electron.[1−23] Because the electron injected into water is fully relaxed within a few picoseconds, femtosecond pump−probe spectroscopy has been performed with use of two-[1−13,23] or three-pulse sequences.[14−22] The absorption signal of a precursor of the fully relaxed electron was first observed in 1987,[1] whereas its existence had been predicted based on the picosecond time-resolved experiments in alcohols.[24−27] The assignment of this precursor as well as its relaxation dynamics has been intensively discussed. Actually, the assignments proposed so far are classified into the following three categories: (1) the precursor is the excited p state;[1−4,6,7] (2) both the p and s states contribute to the absorption band in the femtosecond region;[5,8,14,15] and (3) the precursor is attributable solely to the s state.[9−13,18,21,22] Concerning the spectral evolution, a broad absorption band appears in the near-infrared region after photoionization, and it subsequently shifts to the higher energy side in the femtosecond region until it becomes identical with the fully relaxed band centered at 720 nm. The following three different explanations have been given for this dynamic peak shift: (i) the internal conversion from the p state to the s state;[1−4,6,7] (ii) the stepwise p → s relaxation coupled with the spectral shift due to the solvation;[5,8,14,15] and (iii) the continuous shift attributable to either thermalization[12,21,22] or solvation[9−11,13,18] in the ground state. Recently, the absorption spectrum of the earlier precursor has been observed in the mid-infrared region.[23] Ultrafast time-resolved absorption spectroscopy has played a crucial role in the study of the generation and relaxation dynamics of the hydrated electron. However, it is still difficult to make unambiguous assignments of ultrafast relaxation dynamics of the hydrated electron only on the basis of the time-resolved absorption data.

Recently, we reported resonance Raman scattering from the equilibrated hydrated electron.[28,29] Tauber and Mathies also reported the same phenomena, independently.[30−32] It was found that the intensity of the vibrational Raman bands of the water molecules around the electron is strongly enhanced under the resonance condition with the electronic transition of the hydrated electron. The observed resonance enhancement arises from the strong interaction between the electronic state of the electron and the vibrational state of solvating water molecules. This finding indicates that the hydrated electron should be regarded as a "quasi-molecule" that consists of both the electron and solvating water molecules, and it is too simple to consider it merely as the captured electron in a cavity. The Raman excitation profiles were measured and it was concluded that the s → p transition primarily contributes to the resonance

* Author to whom correspondence should be addressed. E-mail: tahei@riken.jp. Fax: +81-48-467-4539.

† Present address: Molecular Photoscience Research Center, Kobe University, 1-1 Rokkodaicho, Nada-ku, Kobe, Hyogo 657-8501, Japan.

10.1021/jp050828d CCC: $30.25
Published on Web 05/25/2005

enhancement. The observed Raman frequencies of the water molecules that interact with the electron were well reproduced by a recent theoretical calculation for hydrated-hydronium clusters, which is a finite-size model of the hydrated electron in the liquid phase.[33] Therefore, Raman spectroscopy is a new tool to study both the local solvation structure and the nature of the resonant electronic transition of the hydrated electron. It can provide unique information that cannot be obtained by time-resolved absorption measurements.

It is desirable to apply time-resolved Raman spectroscopy to the study of the ultrafast relaxation dynamics of the hydrated electron. However, picosecond time-resolved Raman spectroscopy, which we used to study the equilibrated hydrated electron, cannot provide sufficient time resolution for the dynamics of interest, because the relaxation of the hydrated electron is completed in a few picoseconds. Therefore, we decided to use femtosecond pulses to measure time-resolved resonance Raman spectra for the study of ultrafast relaxation of the hydrated electron. It should be noted that femtosecond time-resolved spontaneous Raman measurements are not usually performed. This is because the broad bandwidth of femtosecond pulses makes the observed Raman bands broad, so that we cannot obtain well-resolved vibrational spectra. In the case of water, however, femtosecond pulses (longer than a few hundred femtoseconds) can provide reasonable spontaneous Raman spectra, because the water Raman bands are isolated and intrinsically broad. The broad bandwidth of femtosecond pulses does not drastically degrade the spectrum.

In this paper, we report femtosecond time-resolved resonance Raman study of the hydrated electron. We examine the temporal intensity changes of the resonance Raman bands of the intra- and intermolecular vibrations of solvating water molecules, and compare them with the change of the luminescence and the transient absorption signals. Anti-Stokes Raman scattering from the hydrated electron is also discussed. Taking advantage of the resonance Raman spectroscopy, we elucidate the nature of the electronic transition of the precursor state of the hydrated electron, from a viewpoint different from that of the time-resolved absorption studies.

2. Experimental Section

The light source of the apparatus was a femtosecond mode-locked Ti:sapphire oscillator (Spectra-Physics, Tsunami) pumped by the frequency-doubled output of a CW diode-pumped Nd:YVO_4 laser (Spectra-Physics, Millennia-Vs). The output of the oscillator laser was amplified with a Ti:sapphire regenerative amplifier (Spectra-Physics, Spitfire) that was pumped by a CW Q-switched, diode-pumped Nd:YLF laser (Spectra-Physics, Evolution-X). The wavelength, pulse energy, pulse width, and repetition rate of the amplified output were 800 nm, 950 μJ, 140 fs, and 1 kHz, respectively. The third harmonic (267 nm) of a part of the amplified output was used as the pump pulse to photoionize water molecules. The residual fundamental output was used as the probe light source. Two probe wavelengths, 800 and 600 nm, were used to obtain the transient Raman signal. The 800-nm probe pulse was the fundamental output of the Ti:sapphire laser. The 600-nm probe pulse was the second harmonic of the signal output of an optical parametric amplifier (Topas, Quantronix) that was pumped by the fundamental output of the regenerative amplifier. The pump and probe pulses were collinearly focused onto a thin film-like jet stream of water (thickness $\sim$300 μm) with a quartz lens ($f = 400$ mm). To minimize the chromatic aberration, the beam radius of the probe pulse was expanded by a lens pair ($f = -250$, 350 mm) before the superimposition of the two pulses. Typical pulse energy was 10 μJ (pump), 2 μJ (800-nm probe), and 0.5 μJ (600-nm probe) at the sample point. The beam radii of the pump and probe pulses were about 200 and 30 μm, respectively. The linear polarizations of the pump and probe pulses were set perpendicular. The zero-delay time was precisely determined by measuring the optical Kerr signal of *n*-hexane. The Raman scattering light was collected and introduced into a spectrometer (Jobin-Ybon, HR320) by a camera lens. A holographic notch filter (Kaiser Optical Systems, Inc.), sharp-cut colored glass filters (HOYA), and a short wave pass dielectric filter (Asahi Spectra Co., Ltd.) were placed before the entrance slit of the spectrometer to eliminate unwanted light, such as strong Rayleigh scattering or the emission arising from the pump pulse irradiation. A liquid nitrogen cooled CCD camera (Princeton Instruments, LN/CCD-1100PB) was used to detect the Raman scattering. The obtained signal intensity, which was distorted by the optics such as a camera lens and filters and by the sensitivity of each pixel on the CCD camera, was corrected by a calibrated halogen lamp (Ushio Inc.).

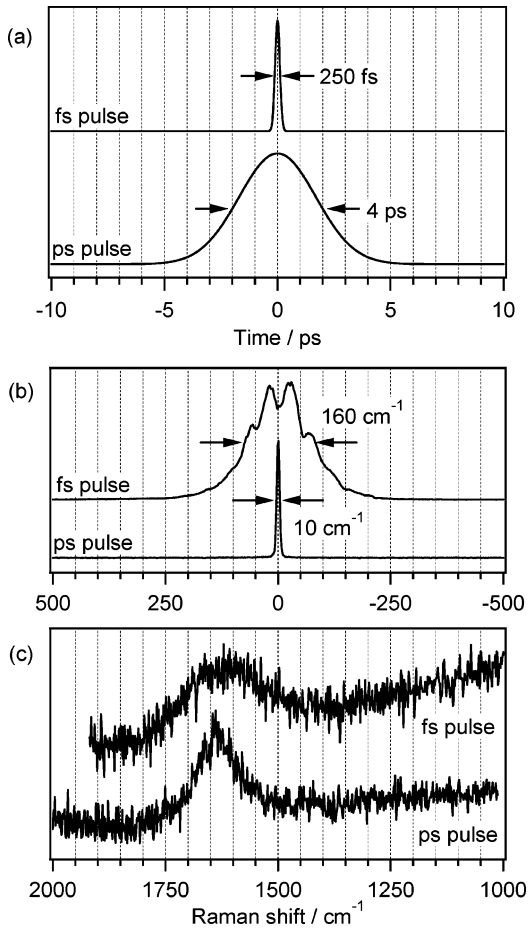

Figure 1. Time traces and spectra of femtosecond and picosecond laser pulses: (a) the cross correlation between the pump and probe pulses; (b) spectra of the probe laser; and (c) Raman spectra of water. The top of each figure represents the data for femtosecond pulses, and the bottom is for picosecond pulses. Probe and pump wavelengths are 800 and 267 nm, respectively.

In Figure 1, the time and spectral resolutions of the present femtosecond setup were compared with those of the picosecond setup that was used in our previous work.[28,29] The time resolution of the measurement (the fwhm of the cross correlation between the pump and probe pulses) was improved from 4 ps to 250 fs, whereas the spectral resolution (the bandwidth of the probe) was significantly lowered from 10 to 160 cm^{-1}.

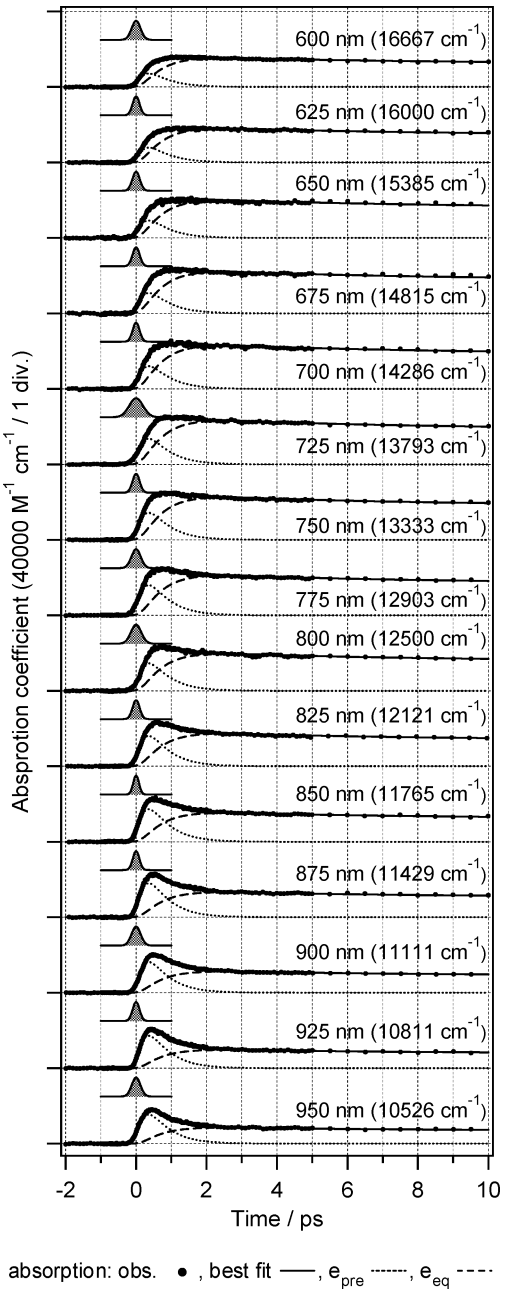

Figure 2. Femtosecond time-resolved absorption traces of the hydrated electron in neat water (dots). The gray filled Gaussian trace denotes the cross correlation between the pump and probe pulses. The black solid line represents the best fitted curves of the transient absorption. The dotted and dashed lines are the contributions of the precursor (e_{pre}) and equilibrated (e_{eq}) states of the hydrated electron, respectively, which were calculated based on formula 2. The pump wavelength is 267 nm. The probe wavelength (as well as the corresponding wavenumber) is indicated for each trace in the figure.

Nevertheless, reasonable Raman spectra can be measured with the present femtosecond setup, as shown in Figure 1c, because the Raman band of water is isolated and intrinsically broad.

Time-resolved absorption traces were measured by monitoring the intensity of the probe pulse that passed through the sample solution. The pump wavelength was 267 nm and the probe light was tuned to 15 wavelengths in the range of 600−950 nm. The probe light was the fundamental output of the regenerative amplifier, the second harmonic of the signal (600−800 nm), or idler (825−950 nm) outputs of the optical parametric amplifier. The measurement was carried out with the same optical setup of the time-resolved Raman measurement. Typical pulse energy was 10 μJ (pump) and <0.1 μJ (probe) at the sample point.

To compare the dynamics measured in time-resolved absorption and time-resolved Raman measurements, we carefully checked the pulse energy dependence of the transient absorption signals. Although some saturation (above the pump energy of 5 μJ) and bleaching (above the probe energy of 0.1 μJ) effects were recognized, no distortion was discerned for the dynamics up to the experimental condition of time-resolved Raman measurements (pump 10 μJ; probe 2 μJ). Therefore, the dynamics of the transient signals measured in time-resolved Raman and absorption measurements can be directly compared to each other.

Distilled water (HPLC grade) was purchased from Wako Pure Chemical Industries and used as received. All measurements were performed at room temperature in the aerated atmosphere.

3. Results and Discussion

3.1. Time-Resolved Absorption. As the basis for discussion on time-resolved Raman data, we first measured femtosecond time-resolved absorption traces and analyzed the kinetics of the absorption data. Time-resolved absorption traces of the hydrated electron monitored at 15 probe wavelengths are shown in Figure 2. Because the two-photon energy of the 267-nm pump light is larger than the ionization threshold of the water molecule (~8.0 eV),[34] the hydrated electron was generated via the two-photon ionization of water in the experiment. The average transient absorbance measured in the range of 20−40 ps (not shown) has been normalized to the extinction coefficient of the equilibrated hydrated-electron [35] at each wavelength.

We analyzed the kinetics of the temporal intensity change of the transient absorption, assuming the following model for the relaxation dynamics:[7]

$$e_{mid-IR} \xrightarrow[\tau_1]{} e_{pre} \xrightarrow[\tau_2]{} {}^{\alpha}\!\rightarrow e_{eq}^{gr}\ \text{(geminate recombination)}$$
$$\xrightarrow{(1-\alpha)} e_{eq}^{long}\ \text{(long-lived species, ~300 ns)} \qquad (1)$$

where e_{mid-IR} is the earlier precursor giving rise to a mid-infrared absorption,[23] e_{pre} represents the precursor of the equilibrated hydrated electron which shows the near-infrared absorption band, e_{eq}^{gr} stands for the equilibrated electron that is going to recombine geminately, e_{eq}^{long} denotes the equilibrated electron that escapes from the geminate recombination, and α is the probability of the geminate recombination. When the electron is injected into water, e_{pre} is generated with the time constant τ_1 from the earlier precursor. In this model, it was assumed that the relaxation process from e_{pre} to the equilibrated state (e_{eq}) is represented by the single-exponential function with the time constant of τ_2. A part of the equilibrated electron decays with the geminate recombination in the picosecond region (e_{eq}^{gr}), and the corresponding population decay is represented by the diffusive model. Consequently, the differential equation for the population change of each state can be written as follows,

$$e_{mid-IR}: \quad \frac{d[e_{mid-IR}]}{dt} = -\frac{[e_{mid-IR}]}{\tau_1} \qquad (2A)$$

$$e_{pre}: \quad \frac{d[e_{pre}]}{dt} = \frac{[e_{mid-IR}]}{\tau_1} - \frac{[e_{pre}]}{\tau_2} \qquad (2B)$$

$$e_{eq}: \quad [e_{eq}] = [e_{eq}^{long}] + [e_{eq}^{gr}]$$

$$\frac{d[e_{eq}^{long}]}{dt} = (1-\alpha)\frac{[e_{pre}]}{\tau_2}$$

$$\frac{d[e_{eq}^{gr}]}{dt} = \alpha\frac{[e_{pre}]}{\tau_2} - [e_{eq}^{gr}]\frac{d}{dt}\,\mathrm{erf}\sqrt{\frac{T}{t}} \qquad (2C)$$

Here, T indicates the jump rate of the one-dimensional random walk model, which is often utilized to numerically describe the recombination between the radical pair in the framework of the diffusion controlled model.[36] Only e_{pre} and e_{eq} give rise to the transient absorption signal in the observed wavelength region. The global fitting for the obtained 15 transient-absorption traces was carried out for these two species on the basis of the kinetics described in formula 2. We fixed the parameter τ_1 at 200 fs, which was the value reported by a time-resolved absorption measurement carried out with 50-fs time resolution,[9] and the other parameters (τ_2, α, T, and extinction coefficients of e_{pre} and e_{eq} at each wavelength) were determined by the fitting. The results of the fitting analysis are shown in Figure 2. The best-fit global parameters were $\tau_2 = 540$ fs, $\alpha = 0.41$, and $T = 3.1$ ps. The wavelength-dependent temporal absorption change in the early delay time reflects the difference in relative extinction coefficients of e_{pre} and e_{eq} at each wavelength. Note that the present model 1 is just for the sake of convenience and it does not necessarily mean a stepwise relaxation process such as the electronic relaxation. Actually, the time constant of τ_2 obtained by the analysis based on model 1 is consistent with the correlation time reported in a previous time-resolved absorption study, in which the dynamic peak shift of the hydrated-electron absorption was assigned not to the stepwise process but to a continuous blue shift.[9] Therefore, the calculated rise time, τ_2, can represent the appearance of the equilibrated hydrated electron, regardless of the assignment of the precursor state of the hydrated electron.

3.2. Time-Resolved Resonance Raman Spectra. We measured femtosecond time-resolved Raman spectra using 267-nm pumping and 800-nm probing. For quantitative discussion on the temporal change of the observed Raman signals, we carefully corrected spectral distortion due to the reabsorption effect of the hydrated electron, using the correction curve created in a way described in the Appendix. Figure 3a shows time-resolved Raman spectra obtained after the correction for the reabsorption effect. We note that the 800-nm light for probing is resonant with not only the electronic transition of the equilibrated electron but also its precursor.[1−13] As seen in the figure, the signal appeared within a few hundreds of femtoseconds after photoionization in both lower (Stokes) and higher energy (anti-Stokes) sides of the probing light (12500 cm^{-1}). Temporal change of the signal was successfully time-resolved with a time resolution as high as 250 fs. The observed signal consists of the Raman scattering and a broad structureless luminescence. The bands around 1600 and 600 cm^{-1}, which are recognized on the luminescence background, are assignable to the intramolecular HOH bending vibration and the intermolecular libration, respectively, of the water molecule that solvates the electron.[28−30,32] The measurement did not cover the region of the OH stretch region (~3200 cm^{-1}) because of lack of the CCD sensitivity.

To separate the Raman band from the luminescence background, we measured time-resolved Raman spectra by slightly shifting the probe wavelength. As the probe wavelength is changed, Raman bands shift correspondingly whereas the luminescence band does not. We measured the time-resolved

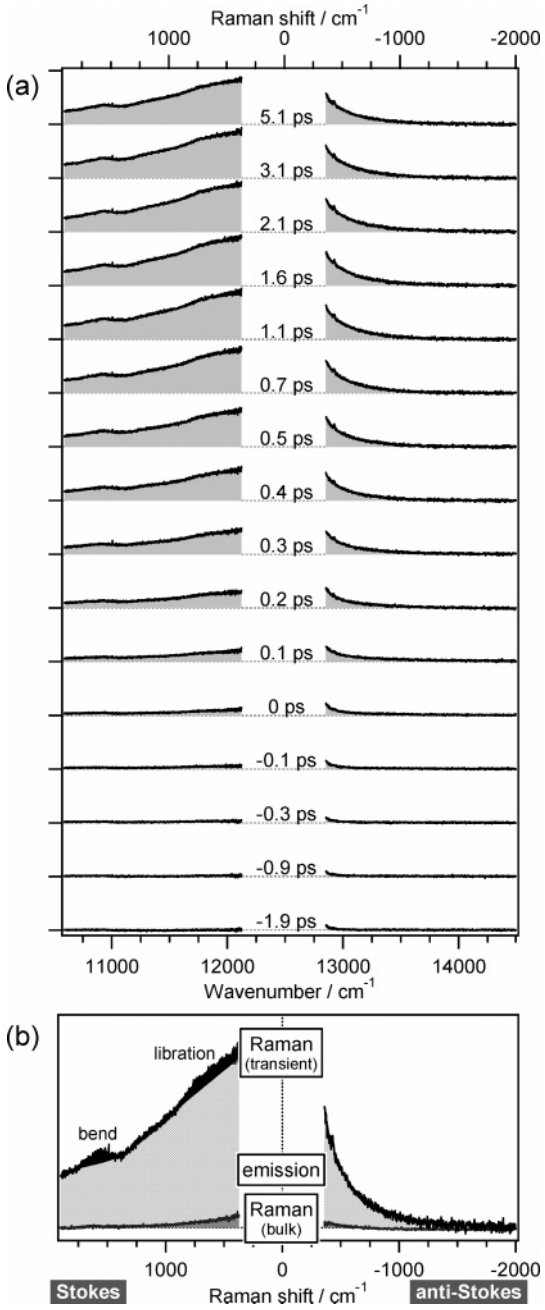

Figure 3. (a) Femtosecond time-resolved spectra of the hydrated electron in the delay time from −1.9 to 5.1 ps (pump laser 267 nm; probe laser 800 nm). The spectrum taken only with pump or probe pulse irradiation has been subtracted from each spectrum, and the spectral distortion due to the reabsorption effect has been corrected. (b) The time-resolved spectrum at 5.1 ps, which is decomposed into each component (see text). The steady-state Raman spectrum of the bulk water is also shown.

Raman spectra with probe at 780 nm and determined the shape of the luminescence background by comparing the data taken with 800-nm probe. In Figure 3b, as an example, the transient spectrum at 5.1 ps was decomposed to Raman scattering and luminescence. By subtracting the luminescence background from the time-resolved spectrum at each delay time, we obtained the femtosecond time-resolved Raman spectra shown in Figure 4.

3.3. Temporal Change of the Raman, Luminescence, and Absorption Signals. We analyzed the temporal intensity changes of the two Stokes Raman bands (bend and libration) and luminescence signal, and plotted them in Figure 5. Because the Raman and luminescence signals from the equilibrated

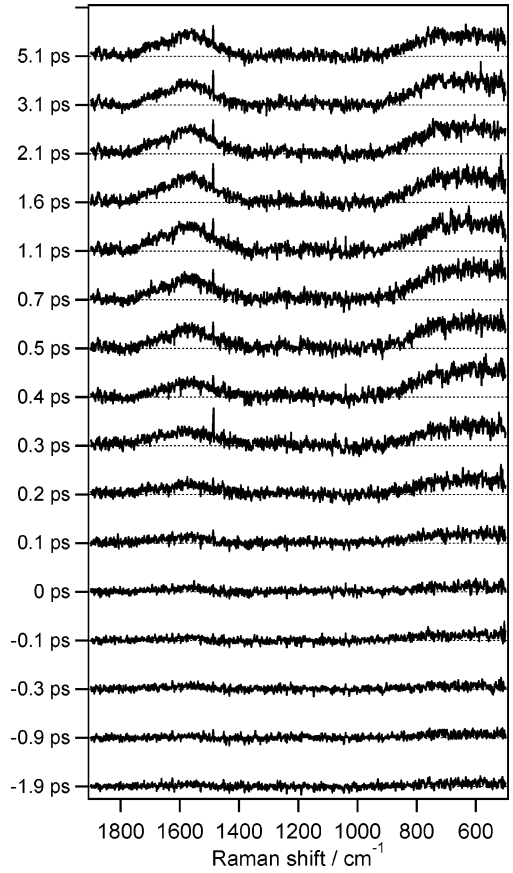

Figure 4. Femtosecond time-resolved resonance Raman spectra of the hydrated electron in the delay time range from −1.9 to 5.1 ps (pump laser 267 nm; probe laser 800 nm). The spectrum taken only with pump or probe pulse irradiation has been subtracted from each spectrum, and the spectral distortion due to the reabsorption effect has been corrected. The luminescence spectrum measured at each delay time has also been subtracted.

hydrated electron originate from the same electronic transition,[30] they exhibit the same temporal behavior after equilibration of the electron. Similarly, the Raman and luminescence signals exhibited the same temporal behavior in early delay time when the relaxation process of the hydrated electron takes place, as shown in Figure 5a−d. We carried out the fitting for the temporal intensity change of these signals based on formula 2, as done for the absorption data. The parameter τ_2, α, and T were fixed at the optimized values for the time-resolved absorption data, because it is known that the equilibrated hydrated electron gave the resonance Raman, luminescence, and absorption signals and hence they should show the same temporal behavior after equilibration.[37] All the traces shown in Figure 5a−d were well fitted with the same fitting parameter τ_1 (∼330 fs), which confirmed that the Raman and luminescence signals behave in the same way also in early delay time when the precursor of the hydrated electron is the dominant species.

Although the temporal behaviors of the transient Raman and luminescence signals are identical, they are different from that of transient absorption in the early delay time. The temporal behavior of the Raman band due to the bending vibration is compared with the time-resolved absorption trace monitored at 800 nm in Figure 6a. Because the temporal behaviors of the libration Raman band and the luminescence signal are identical with that of the bend Raman band, we only show the plot for the bend Raman band here. In the same figure, we also plot the curve that corresponds to the appearance of the equilibrated

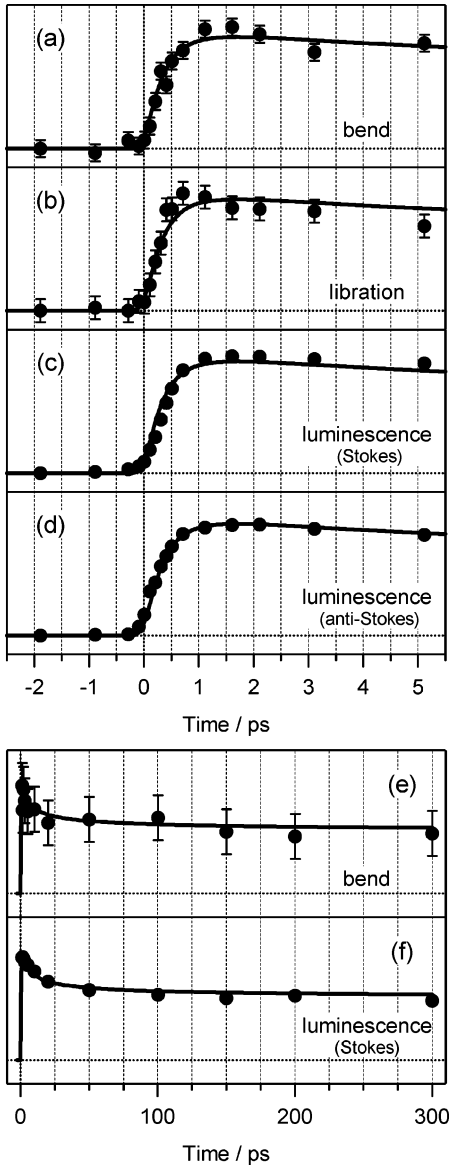

Figure 5. Temporal intensity change of the Stokes Raman bands (bend and libration) and the luminescence (pump laser 267 nm; probe laser 800 nm): (a and e) the Raman intensity due to the intramolecular bend mode (the area intensity from 1450 to 1750 cm^{-1} in Raman shift); (b) the Raman intensity due to the intermolecular libration (the area intensity from 600 to 800 cm^{-1} in Raman shift); (c and f) the luminescence signal observed in the Stokes side (the area intensity from 1000 to 1200 cm^{-1} in Raman shift); and (d) the luminescence signal observed in the anti-Stokes side (the area intensity from −800 to −400 cm^{-1} in Raman shift). The data in the early time region of −2.5 to 5.5 ps are shown in parts a−d, and those in the later time region up to 300 ps are in parts e and f. Filled circles indicate the data point and the solid curves are the best fits based on formula 2. Error bars shown in the figure were determined by the S/N ratio of the obtained spectra.

electron calculated in section 3.1 (the dashed curve). As is clearly seen, (1) the rise time of the Raman bands is faster than the appearance of the equilibrated hydrated electron and (2) it is slower than the rise of the transient absorption signal at the probe wavelength of 800 nm. Because the temporal behavior of the transient Raman and absorption are identical in the long delay time range of 3−300 ps (Figure 6b), this deviation in the femtosecond time range is not an artifact but is inherent to the relaxation process of the hydrated electron.

The transient Raman band due to the solvating water molecule (as well as luminescence) rose faster than the appearance of the equilibrated hydrated electron. It means that the resonance

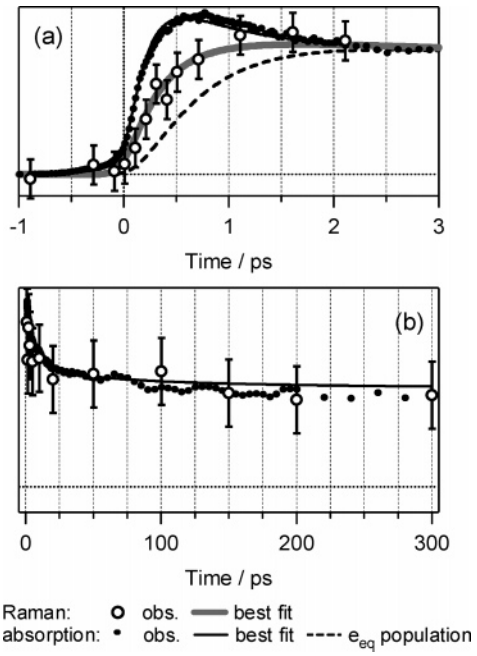

Figure 6. Comparison of the temporal intensity change between transient absorption monitored at 800 nm (black dots) and transient Raman band due to the bend mode probed at 800 nm (open circles). (a) Temporal behavior in the early delay time region of −1 to 3 ps. Thin black and thick gray lines indicate the best-fit curve for the Raman and absorption intensities, respectively. The black dashed line represents the appearance of the equilibrated hydrated electron. (b) Temporal behavior in the later time region up to 300 ps. The black line indicates the population change of the hydrated electron determined by the global fitting for transient absorption.

Raman signals were generated not only from the equilibrated hydrated electron but also from its precursor. In other words, we observed resonantly enhanced Raman scattering also from the water molecules that solvate the precursor-state electron, in the early femtosecond region. In the previous paper, we examined Raman excitation profiles and concluded that the Raman intensity of the water molecules solvating the electron is enhanced under the resonance condition with the s → p transition.[28] The resonance Raman enhancement significantly depends on the electronic transition in resonance. Therefore, the fact that the precursor state also gives a strong resonance Raman signal indicates that the resonant electronic transition of the precursor also has the s → p nature, even though the absorption spectrum is red-shifted. It means that the precursor state of the equilibrated hydrated electron is also the nonequilibrated s-state electron. Consequently, the present Raman study supports (3) and (iii) in the assignments described in the Introduction: the precursor is attributable to the ground-state electron that has higher energy than the fully relaxed one (the nonequilibrated state), and the spectral change of the time-resolved absorption spectra in the femtosecond region is described as a continuous blue shift.[9−13,18,21,22]

It was also found that the rise of the transient Raman band was slower than that of the transient absorption, which was quantitatively confirmed by the fitting analysis resulting in longer τ_1 for the Raman signals (∼330 fs) than for the absorption (200 fs). It implies that, in the delay time range of 0−1.5 ps, the precursor (i.e., the nonequilibrated hydrated electron) absorbs the probe light but does not give rise to the resonance Raman and luminescence signals as much as expected from the absorption intensity. For the equilibrated state, theoretical and experimental studies clarified that the s → conduction band (CB) transition contributes to the blue side of the absorption band, although the main part is ascribed to the s → p transition.[19,20,38] In the previous paper, we reported that the vibrational Raman bands of the solvating water molecules gain very little intensity enhancement when the probe wavelength is tuned to the blue side of the absorption where the contribution of the s → CB transition is significant.[28] The absorption of the nonequilibrated hydrated electron is red-shifted compared to that of the equilibrated electron. Therefore, the probe wavelength at 800 nm is located at the relatively blue side of the transient absorption in the early delay time. Therefore, we consider that, when the transient absorption is largely red-shifted, the 800-nm light probes the blue part of the absorption that gives little resonance Raman intensity (as well as little luminescence intensity), which made the rise curve slower than that of the transient absorption. In other words, we observed the temporal change of the Raman excitation profiles while the transient absorption shows a blue shift during the relaxation process of the hydrated electron. The present observation indicates that the transition energy between the s state and the conduction band as well as the energy between the s and p states increases with time. A theoretical study suggested that only one bound state (the s state) can exist when the solvation structure radius is smaller than a critical value.[39] There might be a short period when the s → p transition itself does not exist in the very early time immediately after photoionization.

The luminescence intensity displayed the same temporal behavior as the Raman intensity, which suggests the luminescence is very weak with the s → CB excitation. This observation leads us to consider that the luminescence also has transition-specific intensity. The luminescence is substantially observed only with the s → p excitation, and therefore luminescence signal from the nonequilibrated state is also attributable to the fluorescence from the p state. The luminescence intensity is small in the case of the s → CB excitation, probably because the electron is detrapped from the solvent cavity.[18−20]

To confirm the dynamic energy-level shift of the hydrated electron as the origin of the delayed appearance of transient Raman and luminescence signals, we measured femtosecond time-resolved Raman and luminescence spectra with 600-nm probe and compared their temporal behavior with transient absorption. The temporal intensity changes of the transient absorption and transient Raman band (the bend mode) measured with two probe wavelengths (800 and 600 nm) are compared in Figure 7. Because the temporal behavior of the luminescence signal was identical with that of the resonance Raman signal, we only show the resonance Raman data here. Also in the case of the 600-nm probe, the rise time of the resonance Raman signal is faster than the appearance of the equilibrated electron but slower than that of the transient absorption. (Note that the absorption signal monitored at 600 nm rose more slowly than the absorption at 800 nm because of the temporal blue shift of the transient absorption.) Moreover, the rise time of the resonance Raman band (τ_1) was different between the 800- and 600-nm probe conditions. They are approximately 330 (800 nm) and 500 fs (600 nm) as shown in Figure 7b. This is consistent with the "dynamic excitation profile" effect. The higher energy probe monitors the blue side of the shifting transient absorption until a later time.

Finally, we mention the anti-Stokes side of the time-resolved Raman spectra. Time-resolved anti-Stokes Raman spectroscopy is a good probe to monitor the local temperature change, because the intensity ratio between the Stokes and anti-Stokes bands is equal to the Boltzmann factor. Keeping this advantage in our

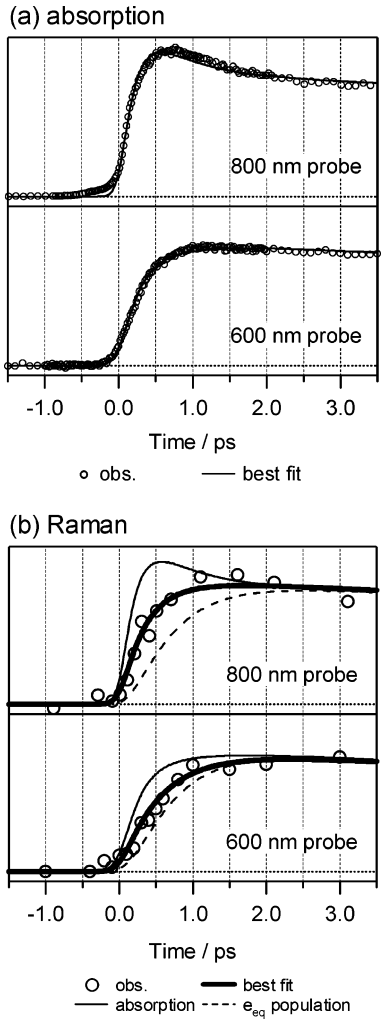

Figure 7. (a) The probe wavelength dependence of the temporal intensity change of the time-resolved absorption (small open circles). Solid lines represent the best-fit curves based on formula 2. (b) The probe wavelength dependence of the temporal intensity change of the resonance Raman band due to the bend mode (large open circles). Thick solid lines indicate the best-fit curves based on formula 2. For comparison, the temporal change of the absorption signal (thin solid lines) and the rise of the equilibrated hydrated-electron population (dashed lines) are also shown. The probe wavelength for each trace is indicated in the figure.

mind, we tried to examine the thermal relaxation dynamics of the nonequilibrated hydrated electron. However, as shown in Figure 3, the signal corresponding to the anti-Stokes Raman bands was not observed even in the early delay time. Taking the S/N ratio of the observed spectra into consideration, we estimated that anti-Stokes Raman intensity is less than 10% of the corresponding Stokes signal. When the intensity ratio between the Stokes and anti-Stokes bands at 0.3 ps is assumed to be 10%, the temperature rise from room temperature is estimated at ∼100 K for the libration band, and ∼700 K for the bend band. Therefore, the local temperature rise of the solvation structure around the electron is less than 100 K already at 0.3 ps. This suggests that the electron injected into water does not excite the water molecule to the vibrationally hot states that can give rise to significant anti-Stokes Raman intensity for the libration as well as the bend mode.

Because the energy for the 100 K temperature rise of a water molecule corresponds to ∼630 cm^{-1},[40] it is roughly considered that the water molecules in the first solvation shell (consisting of ∼6 water molecules[28,29]) hold the thermal energy of less than

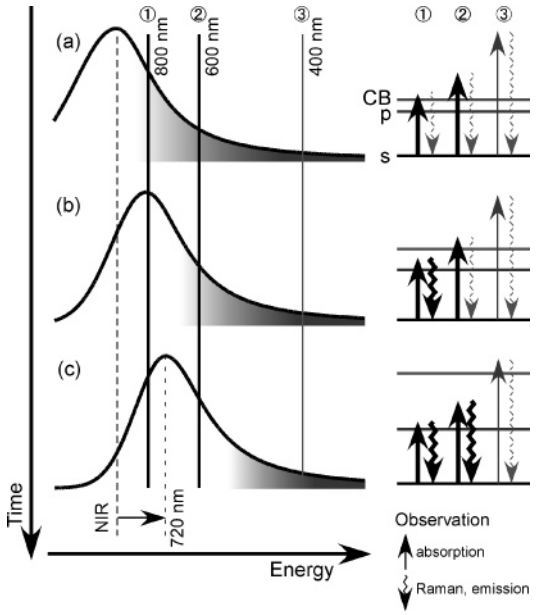

Figure 8. A sketch for the temporal changes in the transient absorption and the electronic transition of the hydrated electron during the relaxation process. Left: The transient absorption spectra of the hydrated electron, in which the gray area indicates the contribution of the s → conduction band (CB) transition. Right: The energy level of the hydrated electron during the relaxation process and the optical process relevant to the present experiments. Three typical probe wavelengths are indicated in the figure: ①, 800 nm, ②, 600 nm, and ③, 400 nm.

∼3780 cm^{-1} at the delay time of 0.3 ps. The initial excess energy of the electron ejection, i.e., 2-photon ionization energy minus the ionization threshold of the water molecule,[34] is calculated at ∼10 400 cm^{-1}. Therefore, a significant amount of energy is distributed over other places than the first solvation shell that gives rise to the resonance Raman signal. We consider that the excess energy can be consumed through the collision with water molecules in the electron ejection path (the average electron ejection distance in the case of about 9-eV 2-photon ionization was evaluated at ∼1.5 nm[10,13]) and the energy is distributed over a larger region. A part of the excess energy may remain in a photoionized water molecule.

Figure 8 sketches the ultrafast relaxation process of the hydrated electron observed in the present Raman study. After photoionization of water, the precursor of the equilibrated hydrated electron (the nonequilibrated ground s-state) is formed. For this state, the s → CB transition contributes to the absorption even at 800 nm in early time, so that there exists a period when Raman resonance enhancement is small compared with transient absorption intensity (Figure 8a). It is considered that the energy difference between the s state and conduction band at that time is approximately half compared to that in the equilibrated state. In accordance with the relaxation of the nonequilibrated electron due to the solvation of the surrounding water molecules (conformational change), the transition energy between the s state and conduction band increases (Figure 8b). Then, the 800-nm probe becomes more resonant with the s → p transition of the nonequilibrated electron, and transient Raman and luminescence signals gain high intensity. The energy relaxation of the electron progresses further, until the electron is fully equilibrated in energy (Figure 8c). In the equilibrated state, the s → CB transition mainly contributes to the blue side of the absorption band around 400 nm,[28,38] and strong transient Raman and luminescence signals are observed with both the 800 and 600 nm probes.

4. Conclusion

We applied time-resolved Raman spectroscopy to the study of femtosecond dynamics of the hydrated electron after two-photon ionization of water. It was shown that time-resolved Raman spectroscopy with 250-fs time resolution provided a new insight on the relaxation dynamics of the hydrated electron. Raman scattering as well as the luminescence signal was observed not only from the equilibrated hydrated electron but also from its precursor state. It was concluded that the precursor of the equilibrated hydrated electron is the ground s-state electron, and the s → p transition gives rise to resonance Raman enhancement. The Raman and luminescence signals rose more slowly than the appearance of the transient absorption. This was explained in terms of the "dynamic excitation profile" effect. When the transient absorption shows a blue shift as a function of time, the effective resonance condition changes also as a function of time, and hence a probe wavelength monitors the bluer part of the absorption that gives smaller resonance Raman intensity in early time. Anti-Stokes Raman bands due to the nonequilibrated hydrated electron were not observed, indicating that the local temperature rise of the solvation structure around the nonequilibrated electron is less than 100 K. The present result supports the argument that the femtosecond relaxation process of the hydrated electron is the conformational change of the solvation structure around the ground s-state hydrated electron.

Appendix

The calibration curve ($C(\tilde{\nu};t)$) to correct the reabsorption effect was created in the following way.

First, we reconstructed time-resolved absorption spectrum ($\epsilon(\tilde{\nu};t)$) at the delay time that corresponds to each time-resolved Raman measurement, using the time-resolved absorption data shown in Figure 2. (Note that the abscissa axis of the absorption spectra was represented by wavenumber for the following procedure.) Because the reconstructed absorption spectra had only sparse data points along the wavenumber axis, we obtained smooth spectra by fitting with the Gaussian function.[41] The ordinate axis of the spectra was normalized to the extinction coefficient of the equilibrated electron by referring to the average transient absorbance in the late delay time range (t_{late}) of 20−40 ps.

Second, the concentration of the equilibrated solvated electron ($c_{electron}$) in the Raman measurements was calculated from the transient absorption at the late delay time ($A_{at0°}(\tilde{\nu}_{probe};t_{late})$), which was monitored by the probe beam passing through the sample, by the following formula,

$$c_{electron} = \frac{A_{at0°}(\tilde{\nu}_{probe};t_{late})}{\epsilon(\tilde{\nu}_{probe};t_{late})\cdot L} \tag{A1}$$

The optical path length (L) was separately evaluated to be 300 μm. Then, the absorbance (at various wavenumbers and at various delay times) for the beam passing through the sample was also calculated as,

$$A_{at0°}(\tilde{\nu};t) = \epsilon(\tilde{\nu};t)\cdot c_{electron}\cdot L \tag{A2}$$

Third, we evaluated the effective optical path length for the scattering in the 90° direction. Since Raman scattering was measured in the 90° direction, the magnitude of the reabsorption effect is correlated to the absorbance for the scattering to the 90° direction, $A_{at90°}(\tilde{\nu};t)$, which is represented as,

$$A_{at90°}(\tilde{\nu};t) = A_{at0°}(\tilde{\nu};t)\cdot\frac{L_{eff}}{L} \tag{A3}$$

Here, L_{eff} is the effective optical path length for the scattering to the 90° direction. We could evaluate L_{eff} from the relative Raman intensity (R_0) between the water bend band of the bulk water (in the probe only spectrum) and that of the equilibrated electron (in the pump and probe spectrum at the late delay time). In the previous paper,[29] we have already determined this intensity ratio using the internal intensity standard to calculate the resonance enhancement factor. If we compare this value with the observed intensity ratio (R_{obs}), we obtain the L_{eff} as follows,

$$\frac{R_{obs}}{R_0} = \frac{I_{obs}^{Tr}/I^{bulk}}{I_0^{Tr}/I^{bulk}} = \frac{I_{obs}^{Tr}}{I_0^{Tr}} = 10^{-A_{at0°}(\tilde{\nu}_{bend};t_{late})\cdot(L_{eff}/L)} = 10^{-\epsilon(\tilde{\nu}_{bend};t_{late})\cdot c_{electron}\cdot L_{eff}} \tag{A4}$$

and hence,

$$L_{eff} = \frac{-\log(R_{obs}/R_0)}{\epsilon(\tilde{\nu}_{bend};t_{late})\cdot c_{electron}} \tag{A5}$$

where I_{obs}^{Tr} and I_0^{Tr} stand for transient HOH bend Raman intensity before and after reabsorption correction. Note that the Raman intensity of bulk water (I^{bulk}) is free from the reabsorption effect because it was measured with only probe. Concretely, the intensity ratio at late delay time was $R_{obs}/R_0 = 0.77$ under the present experimental condition ($c_{electron} = 4.3 \times 10^{-4}$ mol dm^{-3}), which gave $L_{eff} = 290$ μm.

Finally, on the basis of the reconstructed transient absorption spectra ($\epsilon(\tilde{\nu};t)$), the hydrated-electron concentration ($c_{electron}$), and the effective optical path length (L_{eff}), the correction curve for the reabsorption effect at each delay time for Raman measurement was calculated numerically, by the following formula,

$$C(\tilde{\nu};t) = \frac{I_{obs}}{I_0} = 10^{-A_{at90°}(\tilde{\nu};t)} = 10^{-A_{at0°}(\tilde{\nu};t)\cdot(L_{eff}/L)} = 10^{-\epsilon(\tilde{\nu};t)\cdot c_{electron}\cdot L_{eff}} \tag{A6}$$

Then, the corrected time-resolved spectra ($S_0(\tilde{\nu};t)$) were obtained from the observed spectra ($S_{obs}(\tilde{\nu};t)$) as follows,

$$S_0(\tilde{\nu};t) = \frac{S_{obs}(\tilde{\nu};t)}{C(\tilde{\nu};t)} \tag{A7}$$

References and Notes

(1) Migus, A.; Gauduel, Y.; Martin, J. L.; Antonetti, A. *Phys. Rev. Lett.* **1987**, *58*, 1559.
(2) Pommeret, S.; Antonetti, A.; Gauduel, Y. *J. Am. Chem. Soc.* **1991**, *113*, 9105.
(3) Long, F. H.; Lu, H.; Eisenthal, K. B. *Phys. Rev. Lett.* **1990**, *64*, 1469.
(4) Shi, X.; Long, F. H.; Lu, H.; Eisenthal, K. B. *J. Phys. Chem.* **1996**, *100*, 11903.
(5) Messmer, M. C.; Simon, J. D. *J. Phys. Chem.* **1990**, *94*, 1220.
(6) Keszei, E.; Murphrey, T. H.; Rossky, P. J. *J. Phys. Chem.* **1995**, *99*, 22.
(7) Reuther, A.; Laubereau, A.; Nikogosyan, D. N. *J. Phys. Chem.* **1996**, *100*, 16794.
(8) Pépin, C.; Goulet, T.; Houde, D.; Jay-Gerin, J. P. *J. Phys. Chem. A* **1997**, *101*, 4351.
(9) Vilchiz, V. H.; Kloepfer, J. A.; Germaine, A. C.; Lenchenkov, V. A.; Bradforth, S. E. *J. Phys. Chem. A* **2001**, *105*, 1711.
(10) Kloepfer, J. A.; Vilchiz, V. H.; Lenchenkov, V. A.; Germaine, A. C.; Bradforth, S. E. *J. Chem. Phys.* **2000**, *113*, 6288.

(11) Lenchenkov, V.; Kloepfer, J.; Vilchiz, V.; Bradforth, S. E. *Chem. Phys. Lett.* **2001**, *342*, 277.
(12) Hertwig, A.; Hippler, H.; Unterreiner, A.-N. *Phys. Chem. Chem. Phys.* **1999**, *1*, 5633.
(13) Madsen, D.; Thomsen, C. L.; Thøgersen, J.; Keiding, S. R. *J. Chem. Phys.* **2000**, *113*, 1126.
(14) Kimura, Y.; Alfano, J. C.; Walhout, P. K.; Barbara, P. F. *J. Phys. Chem.* **1994**, *98*, 3450.
(15) Yokoyama, K.; Silva, C.; Son, D. H.; Walhout, P. K.; Barbara, P. F. *J. Phys. Chem. A* **1998**, *102*, 6957.
(16) Silva, C.; Walhout, P. K.; Yokoyama, K.; Barbara, P. F. *Phys. Rev. Lett.* **1998**, *80*, 1086.
(17) Silva, C.; Walhout, P. K.; Reid, P. J.; Barbara, P. F. *J. Phys. Chem. A* **1998**, *102*, 5701.
(18) Kambhampati, P.; Son, D. H.; Kee, T. W.; Barbara, P. F. *J. Phys. Chem. A* **2002**, *106*, 2374.
(19) Son, D. H.; Kambhampati, P.; Kee, T. W.; Barbara, P. F. *J. Phys. Chem. A* **2001**, *105*, 8269.
(20) Son, D. H.; Kambhampati, P.; Kee, T. W.; Barbara, P. F. *Chem. Phys. Lett.* **2001**, *342*, 571.
(21) Assel, M.; Laenen, R.; Laubereau, A. *J. Chem. Phys.* **1999**, *111*, 6869.
(22) Assel, M.; Laenen, R.; Laubereau, A. *Chem. Phys. Lett.* **2000**, *317*, 13.
(23) Laenen, R.; Roth, T.; Laubereau, A. *Phys. Rev. Lett.* **2000**, *85*, 50.
(24) Miyasaka, H.; Masuhara, H.; Mataga, N. *Chem. Phys. Lett.* **1983**, *98*, 277.
(25) Wang, Y.; Crawford, M. K.; McAuliffe, M. J.; Eisenthal, K. B. *Chem. Phys. Lett.* **1980**, *74*, 160.
(26) Chase, W. J.; Hunt, J. W. *J. Phys. Chem.* **1975**, *79*, 1975.
(27) Kenney-Wallace, G. A.; Jonah, C. D. *J. Phys. Chem.* **1982**, *86*, 2572.
(28) Mizuno, M.; Tahara, T. *J. Phys. Chem. A* **2003**, *107*, 2411.
(29) Mizuno, M.; Tahara, T. *J. Phys. Chem. A* **2001**, *105*, 8823.
(30) Tauber, M. J.; Mathies, R. A. *J. Phys. Chem. A* **2001**, *105*, 10952.
(31) Tauber, M. J.; Mathies, R. A. *Chem. Phys. Lett.* **2002**, *354*, 518.
(32) Tauber, M. J.; Mathies, R. A. *J. Am. Chem. Soc.* **2003**, *125*, 1394.
(33) Neumann, S.; Eisfeld, W.; Sobolewski, A.; Domcke, W. *Phys. Chem. Chem. Phys.* **2004**, *6*, 5297.
(34) Crowell, R. A.; Bartels, D. M. *J. Phys. Chem.* **1996**, *100*, 17940.
(35) Jou, F.-Y.; Freeman, G. R. *J. Phys. Chem.* **1979**, *83*, 2383.
(36) Shank, C. V.; Yen, R.; Fork, R. L.; Orenstein, J.; Baker, G. L. *Phys. Rev. Lett.* **1982**, *49*, 1660.
(37) In the fitting for Raman (luminescence) signals, we set the Raman (luminescence) intensities of e_{pre} and e_{eq} at the same value to reduce the number of adjustable parameters, and evaluated the apparent rise time τ_1.
(38) Schnitker, J.; Motakabbir, K.; Rossky, P. J.; Friesner, R. *Phys. Rev. Lett.* **1988**, *60*, 456.
(39) Tachiya, M. *J. Chem. Phys.* **1978**, *69*, 748.
(40) This value is calculated from the specific heat of the bulk water.
(41) It is known that the whole absorption shape of the hydrated electron is well reproduced by the combination of the Gaussian ($\lambda > \lambda_{max}$) and Lorentzian ($\lambda < \lambda_{max}$) functions along wavenumber according to ref 35. Nevertheless, the probe range of the present absorption measurements was limited around the maximum of the absorption band, and the fitting with only Gaussian function did not cause any noticeable deviation. In fact, the reconstructed smooth Gaussian spectra surely exhibited similar spectral evolution as that reported in ref 9.